Multiscale and Multidisciplinary Modeling, Experiments and Design (2026) 9:171
https://doi.org/10.1007/s41939-026-01254-2

BRIEF COMMUNICATION

Competing surface and geometric effects in the size-dependent vibrational response of hollow silicon nanobeams

Akbar Hassanpour[1] · **Hamid M. Sedighi**[2]

Received: 12 May 2026 / Revised: 28 June 2026 / Accepted: 22 July 2026

Abstract

Classical continuum theories neglect surface-dominated effects that govern the mechanical response of nanostructures at high surface-to-volume ratios (SVR). Using molecular dynamics simulations, this work examines the size-dependent free transverse vibration of solid and hollow silicon nanobeams and shows that hollow geometries exhibit a non-monotonic dependence of natural frequency on cavity size, in contrast to the monotonic surface-induced softening displayed by solid nanobeams. For small cavities, geometric stiffening from the redistribution of material away from the neutral axis outweighs surface softening, increasing the frequency despite a rising SVR; as the cavity enlarges and the walls thin, the negative surface elastic constants of silicon dominate, producing a pronounced frequency drop. This competition is shown to be quantitatively consistent with an extension of the Miller–Shenoy surface-elasticity framework to hollow cross-sections, and is distilled into a minimal two-term dimensionless scaling law that balances a geometric stiffening term against a surface-softening term governed by the ratio of an intrinsic material length scale to the beam's outer dimension. The scaling law predicts the cavity ratio at which the stiffening-to-softening transition occurs, and the molecular dynamics results show this transition at a smaller cavity ratio than the continuum prediction, pointing to an additional, cross-section-dependent atomistic contribution to surface softening not captured by the linear continuum model. These results clarify the competing mechanisms governing the vibrational response of hollow nanobeams and provide a predictive, extensible framework connecting molecular-scale surface elasticity to continuum-level nanoscale design.

✉ Akbar Hassanpour
ahassan@ippt.pan.pl

[1] Institute of Fundamental Technological Research, Polish Academy of Sciences, Pawińskiego 5B, 02-106 Warsaw, Poland

[2] Mechanical Engineering Department, Faculty of Engineering, Shahid Chamran University of Ahvaz, Ahvaz, Iran

Published online: 05 August 2026

Graphical abstract

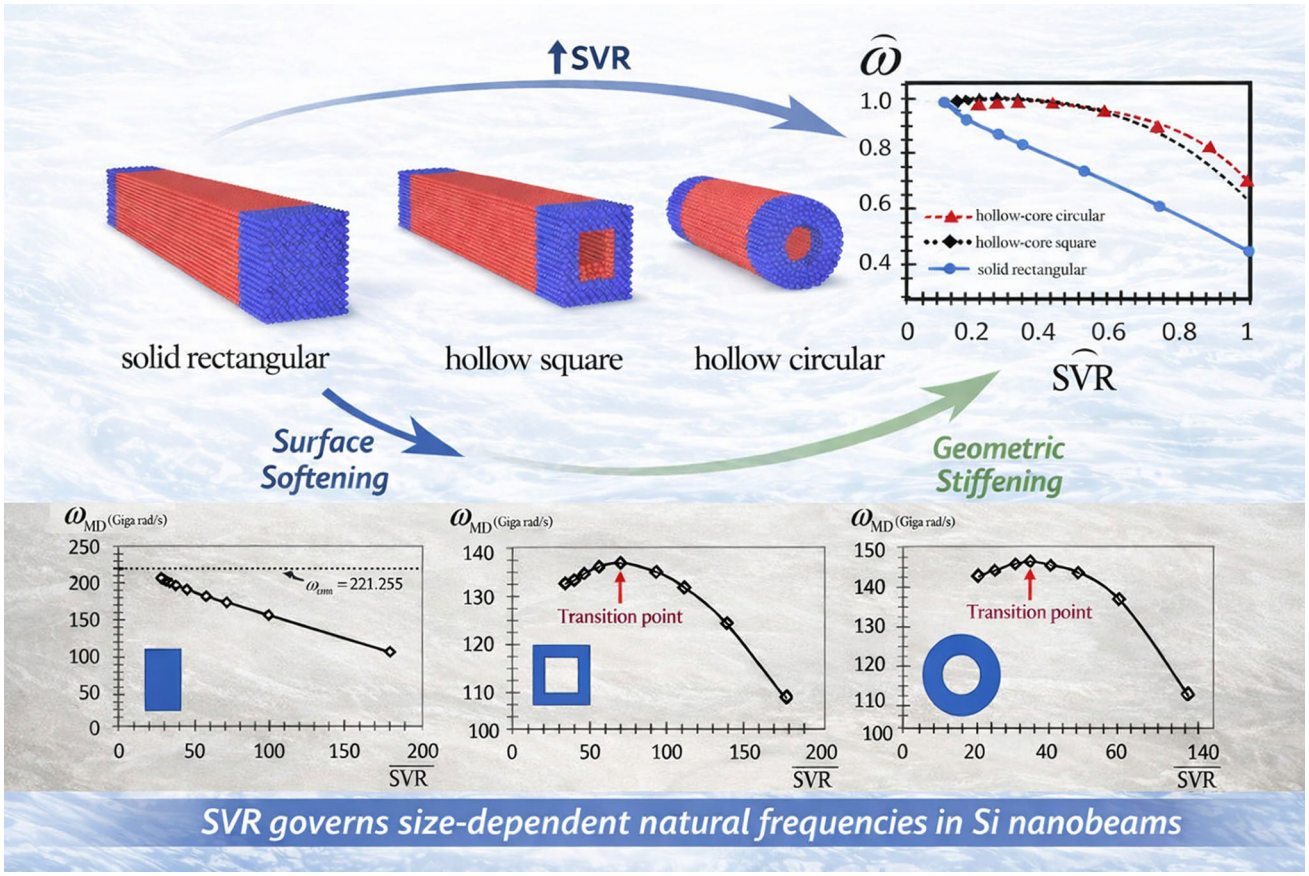

Keywords Hollow nanobeams · Non-monotonic vibration · Surface-to-volume ratio · Size-dependent effects · Molecular dynamics

1 Introduction

At macroscopic scales, the contribution of surface atoms to the overall mechanical response of a structure is negligible because the surface area is extremely small relative to the volume. Classical continuum mechanics therefore assumes size-independent material properties governed entirely by bulk elasticity (Love 1892; Abazari et al. 2015). However, as structural dimensions shrink to the nanometer scale, this assumption becomes invalid (Wong et al. 1997). The substantial increase in the surface-to-volume ratio (SVR) causes surface forces such as van der Waals, capillary, electrostatic, and chemical bonding interactions, to become comparable to body forces, including gravity and inertia (Roduner 2006). As a result, a significant fraction of atoms resides at or near free surfaces, where they experience broken bonds, reduced coordination numbers, and altered electronic environments relative to their bulk counterparts (Cammarata 1994). These surface-dominated effects lead to size-dependent mechanical behavior that deviates from classical continuum predictions (Cammarata 1997; CAO and CHEN 2008; Shariati et al. 2020).

The distinction between surface and bulk atoms forms the basis of surface elasticity theory, initially formalized by Gurtin and his coworkers (Gurtin and Ian Murdoch 1975; Gurtin et al. 1998), who modeled the surface as an independent elastic membrane with its own constitutive behavior. Within this framework, a nanostructure can be conceptually partitioned into a bulk region, composed of fully coordinated atoms that follow classical elasticity, and a surface region of under-coordinated atoms with modified stiffness. The mechanical response of the entire structure therefore depends on how these two regions resist deformation and interact across their interface. Surface elasticity frameworks have been widely applied to small-scale structures to investigate size-dependent mechanical behavior in nanostructures, including nanowires (He and Lilley 2008a, 2008b; Cuenot et al. 2004; Limkatanyu et al. 2025), thin films (He et al.

2004; Dingreville et al. 2005), nanoplates (Wang and Wang 2011; Bochkarev and Grekov 2019; Eremeyev and Wiczenbach 2020), and nanoshells (Altenbach and Eremeyev 2011; Sahmani et al. 2020; Avramov et al. 2024), demonstrating that surface stresses and surface elastic moduli can significantly alter the effective stiffness as structural dimensions decrease.

In an extension of this framework to circular nanoplate geometries, the Gurtin–Murdoch surface elasticity model was coupled with nonlocal theory, and MD simulations were employed to compute the surface residual strain energies at different crystal orientations of copper (Tang et al. 2024). The results demonstrated that surface and nonlocal effects produce significant size-dependent deviations in bending deflection, with the influence becoming negligible only as the plate thickness grows well beyond the intrinsic material length scale. For beam-type structures operating in fluid environments, it was shown that scale corrections based on modified couple stress theory produce notable upward shifts in the resonant frequency and quality factor of functionally graded microcantilever beams when their thickness approaches the material length scale, with the size effect diminishing progressively as the thickness-to-scale ratio increases (Jiang et al. 2025).

A central question in nanoscale elasticity is whether surfaces behave as elastically softer or stiffer layers compared with the bulk. It has been shown that both behaviors are possible, depending on the relative influence of electron density redistribution, which tends to stiffen the surface, and reduced atomic coordination, which tends to soften it (Zhou and Huang 2004). For silicon, atomistic simulations revealed that surface elastic constants may become negative, indicating that the coordination-loss mechanism dominates and that surface layers act as compliant regions that reduce the overall stiffness (Miller and Shenoy 2000). A scaling relation was further proposed to describe the competition between surface and bulk elasticity in simple solid geometries. These findings established silicon as a model material for probing size-dependent elasticity governed by negative surface elastic moduli.

The preceding discussion indicates that the competition between bulk and surface elasticity is fundamentally governed by the relative proportion of surface atoms within a structure. This proportion is most naturally quantified by the SVR, which provides a geometric measure of surface dominance. As structural dimensions decrease or internal cavities are introduced, the SVR increases, amplifying the contribution of surface elasticity relative to bulk elasticity. Therefore, the SVR can be regarded as a fundamental scaling parameter in nanoscale mechanics. The importance of SVR has been demonstrated across multiple physical properties of silicon nanostructures. Molecular dynamics simulations of silicon nanowires with different cross-sectional geometries showed that thermal conductivity decreases monotonically with increasing SVR, establishing SVR as a governing parameter independent of cross-sectional shape (Chen et al. 2011). In a closely related study, the introduction of a central cavity to form silicon nanotubes led to a significant reduction in thermal conductivity compared with solid nanowires, primarily attributed to the increased SVR and enhanced surface phonon localization at the cavity walls (Chen et al. 2010). The influence of SVR has also been observed in the electronic properties of semiconductor nanowires and nanotubes, where first-principles calculations reveal systematic size-dependent variations in band gap arising from surface-state interactions and quantum confinement effects (Pan and Feng 2008). These studies collectively highlight the central role of SVR in governing size-dependent behavior at the nanoscale.

Recent studies on hollow nanostructures have shown that geometric modification can interact with surface-related effects in ways that deviate from classical elasticity, although the reported trends have so far remained strictly monotonic. The vibrational behavior of single-walled ZnO nanotubes was shown to exhibit a monotonic decrease in natural frequency with increasing aspect ratio, attributed to bending–membrane coupling and lattice anisotropy inherent to the tubular geometry (Chowdhury et al. 2011). Similarly, MD simulations of ultrathin ZnO nanowires have demonstrated that axial stiffness and yield strength vary strongly with wire diameter due to surface relaxation and phase-transformation mechanisms, yet the response remains monotonic with respect to size, without any intermediate stiffening regime (Lee et al. 2011). Extensive MD studies of carbon nanotubes have likewise reported diameter-dependent softening or stiffening trends arising from chirality, wall structure, and temperature effects, but again the mechanical response varies monotonically with tube diameter or aspect ratio (Najmi and Hu 2024). The radial vibrational response of single-walled zigzag carbon nanotubes under pulsed external pressure has similarly been analyzed using both shell theory and MD, with the frequency response varying smoothly and monotonically with applied pressure and tube size (Ilgamov et al. 2024). First-principles studies of crystalline SiC nanotubes have similarly revealed pronounced size- and surface-dependent variations in electronic structure driven by quantum confinement and surface states, which nevertheless manifest as smooth monotonic trends rather than non-monotonic transitions (Zhou et al. 2011). Taken together, these studies confirm that while hollow nanostructures across a range of materials exhibit pronounced size-dependent behavior, their responses are typically monotonic either softening or stiffening depending on surface chemistry and geometry rather than displaying a stiffening-to-softening transition of the kind that would arise from a genuine competition between geometric and surface effects.

For silicon specifically, whether the same type of competition can produce a non-monotonic, rather than purely monotonic, vibrational response remains unexplored. Although the monotonic softening of solid silicon nanobeams with increasing SVR is well established, the vibrational behavior of hollow silicon nanobeams remains insufficiently understood, and the possibility of a non-monotonic trend arising from competing geometric stiffening and surface-induced softening distinct from the monotonic trends reported above for hollow nanostructures of other materials has not been systematically explored.

Addressing this gap is particularly relevant given silicon's central role in nanoscale device technology. Silicon nanostructures have been extensively studied because of silicon's dominant role as a structural material in MEMS and NEMS technologies (Bhushan 2017; Zhu et al. 2020; Fu et al. 2025). Silicon nanobeams are widely employed in high performance field effect transistors (Cui et al. 2003), resonators (Craighead 2000; Jiang et al. 2020; Zhang et al. 2025), biological and chemical sensors as well as mass sensors (Anderson et al. 1994; Cui et al. 2001; Langfelder et al. 2021), actuators (Xu et al. 2025), microneedle-based neural infusion systems (Chen et al. 1997; Lee et al. 2018), and logic devices (Huang et al. 2001), where accurate prediction of mechanical characteristics such as natural frequencies is essential for performance and reliability. The mechanical behavior of silicon at the nanoscale has been systematically examined through both experimental studies (Sohn et al. 2009; Sadeghian et al. 2010; Kim et al. 2011; Chen et al. 2020; Zare Pakzad et al. 2021, 2023) and MD simulations (Park et al. 2005; Du et al. 2015; Pakzad et al. 2024; Hassanpour and Darban 2025, 2026), establishing silicon as a model system for investigating size-dependent mechanical properties.

In this work, MD simulations are employed to examine how the SVR influences the free transverse vibration of solid and hollow silicon nanobeams. By systematically varying beam width in solid nanobeams and cavity size in hollow nanobeams, the study isolates the role of geometric modification and surface elasticity in shaping the vibrational response. This approach enables a direct assessment of how bulk stiffness, geometric redistribution of material, and surface-induced effects interact at the nanoscale. The objective is to clarify the competing physical mechanisms governing size-dependent elasticity in silicon nanobeams and to establish a consistent framework for comparing solid and hollow geometries.

The structure of the paper is as follows. Section 2 presents the problem definition, geometric characterization, and MD simulation procedure. Section 3 presents and discusses the results. First, the influence of surface-to-volume ratio on the vibrational response of solid rectangular silicon nanobeams is examined, followed by an investigation of hollow square and hollow circular nanobeams to identify the competition between geometric stiffening and surface-induced softening. The MD results are then compared with the Miller–Shenoy surface-elasticity theory, and a dimensionless scaling law is developed to characterize the transition between bulk-dominated and surface-dominated behavior. Section 4 discusses the limitations of the present study and outlines directions for future research. Finally, Sect. 5 summarizes the main findings and conclusions.

2 Problem definition and assumptions

To investigate the impact of surface-to-volume ratio on the size-dependent free transverse vibration of silicon nanobeams, atomistic models of solid and hollow nanobeams are constructed and analyzed using MD simulations. The objective is to systematically isolate the role of SVR as the governing geometric parameter controlling deviations from classical continuum predictions.

Two classes of nanobeams are considered:

- Solid rectangular nanobeams, where the cross-sectional width is varied while thickness and length are kept constant.
- Hollow nanobeams (square and circular cross-sections), where the outer dimensions and length are fixed, and the inner cavity size is varied.

This strategy allows independent control of the SVR while preserving the overall beam length, thereby enabling direct comparison of vibrational behavior as SVR changes.

For all cases, the natural frequencies of silicon nanobeams obtained from MD simulation (ω_{MD}) are reported together with the corresponding classical Timoshenko beam predictions (ω_{cont}). While ω_{cont} is independent of structural size and derived from continuum mechanics assumptions, ω_{MD} inherently captures nanoscale effects. Therefore, comparing these two quantities enables a quantitative assessment of size-dependent deviations and clarifies how variations in the SVR influence the vibrational response. To further quantify this deviation, the frequency ratio $\left(\frac{\omega_{\mathrm{MD}}}{\omega_{\mathrm{cont}}}\right)$ is calculated for all cases. This ratio directly measures the extent to which the actual nanobeam frequency obtained from MD simulations departs from the corresponding classical continuum prediction, providing a clear metric for evaluating size effects.

2.1 Geometric definition and surface-to-volume ratio

The surface-to-volume ratio (SVR) quantifies the influence of surface effects at the nanoscale and is defined as

$$\mathrm{SVR} = \frac{A_S}{V} \tag{1}$$

where A_S is the total surface area and V is the volume of the nanobeam.

For hollow-core rectangular nanobeams with length L, outer width W_{out}, outer height H_{out}, and inner dimensions W_{in} and H_{in}, the SVR is given by

$$\mathrm{SVR} = \frac{2\left[L(W_{\mathrm{out}} + H_{\mathrm{out}} + W_{\mathrm{in}} + H_{\mathrm{in}}) + (W_{\mathrm{out}}H_{\mathrm{out}} - W_{\mathrm{in}}H_{\mathrm{in}})\right]}{L(W_{\mathrm{out}}H_{\mathrm{out}} - W_{\mathrm{in}}H_{\mathrm{in}})} \tag{2}$$

For hollow-core circular nanobeams with length L, outer diameter D_{out}, and inner diameter D_{in}, the SVR is expressed as

$$\mathrm{SVR} = \frac{4\left[L(D_{\mathrm{out}} + D_{\mathrm{in}}) + \frac{1}{2}(D_{\mathrm{out}}^2 - D_{\mathrm{in}}^2)\right]}{L(D_{\mathrm{out}}^2 - D_{\mathrm{in}}^2)} \tag{3}$$

For all nanobeams considered in this study, the beam length L is kept constant within each comparison group. To facilitate comparison across the considered cases, a dimensionless surface-to-volume ratio is introduced by multiplying the conventional SVR by L, yielding

$$\overline{\mathrm{SVR}} = \mathrm{SRV} \times L \tag{4}$$

This dimensionless parameter depends only on the cross-sectional geometry and provides a convenient dimensionless measure for comparing solid and hollow configurations.

2.2 Molecular dynamics simulations

The MD simulations are performed using the Large Scale Atomic/Molecular Massively Parallel Simulator (LAMMPS) (Plimpton 1995) to study the size-dependent free transverse vibrations of silicon nanobeams with clamped–clamped boundary conditions. The atomic structures are visualized using the Open Visualization Tool (OVITO) (Stukowski 2009). The nanobeams are constructed from single-crystal silicon with a diamond cubic lattice structure and a lattice constant of 0.5431 nm.

Several empirical interatomic potentials have been developed to describe Si–Si interactions, including the Tersoff potential (Tersoff 1988), Stillinger–Weber (SW) potential (Stillinger and Weber 1985), the environment-dependent interatomic potential (EDIP) (Bazant et al. 1997), and the modified embedded atom method (MEAM) potential (Baskes 1992). Among these, the SW potential has been widely used and extensively validated in MD studies of silicon nanostructures, particularly for accurately reproducing elastic properties. Therefore, the SW potential provides a reliable and computationally efficient framework for investigating the mechanical behavior of silicon at the nanoscale.

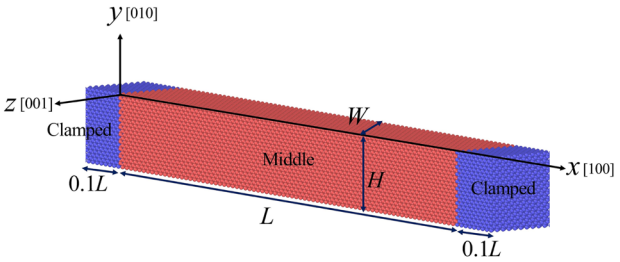

Fig. 1 Atomic configurations of silicon clamped–clamped nanobeams used in the MD simulations

In this study, the SW interatomic potential is employed. This potential is particularly suitable for covalently bonded materials with a diamond cubic structure, such as silicon, as it incorporates both two-body and three-body interaction terms to capture bond stretching and angular dependencies.

To model clamped boundary conditions, finite regions of length $0.1L$ are defined at both ends of the nanobeam. All atomic degrees of freedom within these regions are constrained, preventing both translational and rotational motion. The simulation domain is defined with shrink-wrapped boundary conditions in all spatial directions. The nanobeams are oriented along the [100] crystallographic direction, with the longitudinal axis aligned with the x-direction. Figure 1 shows a representative atomic configuration of the silicon clamped–clamped nanobeams used in the MD simulations.

Prior to dynamic analysis, the atomic structure is relaxed using the conjugate gradient energy minimization method to remove residual stresses and obtain a stable equilibrium configuration. Atomic velocities are subsequently initialized according to a Maxwell–Boltzmann distribution at a target temperature of $T = 1$ K. Conducting the simulations at 1 K minimizes thermal fluctuations of atoms and ensures a stable and reliable evaluation of the intrinsic vibrational behavior. It also enables the isolation of size-dependent effects without interference from thermal noise. The system is then equilibrated under the canonical (NVT) ensemble using a Nosé–Hoover thermostat for 100,000 steps, corresponding to 100 ps with an integration time step of $\Delta t = 1$ fs, after which the thermostat is removed.

After equilibration, atoms in the constrained boundary regions are fixed to enforce the prescribed support conditions, whereas atoms in the deformable middle segment remain fully dynamic. Transverse vibration is initiated by applying an initial displacement in the transverse (y) direction to atoms within the free span. The imposed displacement field follows the analytical first bending mode of a clamped—clamped beam, expressed as

$$u_y(x) = A \sin\left(\frac{x - x_0}{L}\pi\right) \tag{5}$$

where A is the excitation amplitude, x_0 denotes the x-coordinate of the start of the free vibrating span, and $L = x_1 - x_0$ is the length of the free span, with x_1 marking the beginning of the right clamped region. The excitation amplitude is set to $A = 0.002L$. This formulation ensures zero displacement at both clamped ends and a maximum displacement at the midspan. Following the application of this initial excitation, the system is evolved under microcanonical (NVE) dynamics for 250,000 time steps (equivalent to 250 ps) to capture the free vibration response.

To quantify the vibration, the instantaneous out-of-plane displacement of each atom is projected onto the analytical first-mode shape. The generalized modal amplitude at time t is computed as

$$A(t) = \sum_{i=1}^{N} y_i(t)\, \sin\left(\frac{x_i - x_0}{L}\pi\right) \tag{6}$$

where y_i(t) is the transverse displacement of atom i. This modal projection isolates the contribution of the fundamental bending mode and suppresses higher-mode and thermal components, yielding a clean scalar time series representing the dominant structural vibration.

The modal amplitude is sampled at uniform intervals (every 100 time steps), generating a discrete signal $A(t_k)$. A Fast Fourier Transform (FFT) is applied to this signal to obtain its spectral content. For a uniformly sampled signal, the FFT produces complex coefficients

$$\widehat{A}(\omega_j) = \sum_{i=1}^{N} A(t_k)\, e^{-i\omega_j t_k} \tag{7}$$

where ω_j are the discrete angular frequencies associated with the transform. The magnitude spectrum $\left|\widehat{A}(\omega_j)\right|$ exhibits a dominant peak corresponding directly to the first natural angular frequency of the nanobeam. The value of ω_1 is identified as the angular frequency at which the FFT magnitude reaches its maximum.

This FFT-based procedure provides a robust and noise-resistant estimate of the fundamental natural angular frequency, as it relies on modal projection of atomic displacements and spectral decomposition of the resulting time series. The resulting spectrum exhibits a single sharp peak, enabling accurate extraction of the first natural angular frequency of the silicon nanobeams. Figure 2 illustrates the extraction of the first natural frequency of a solid rectangular silicon nanobeam obtained from MD simulations using the described method.

As a complementary approach, the natural frequency can also be extracted by tracking the average y-coordinate of atoms within the excitation region as a function of time, t. The resulting vibration response is fitted to a sinusoidal function, $u_y(t) = A\sin(Bt + C)$, where A, B, and C are fitting parameters. The natural angular frequency is then obtained directly from the fitted parameter B, with $\omega = 10^3 B$, expressed in Giga rad/s.

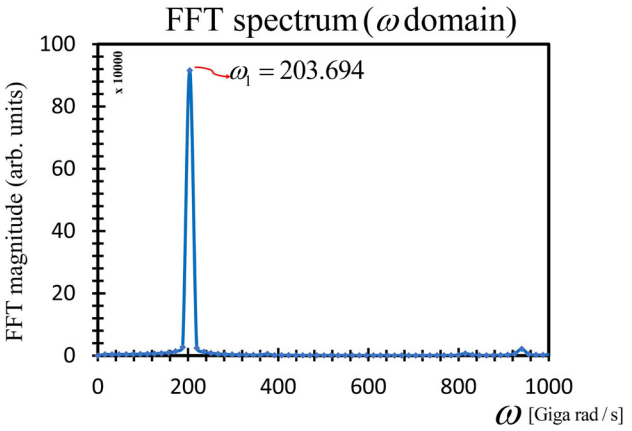

Fig. 2 Determination of the natural frequency of a solid rectangular silicon nanobeam based on MD results. The nanobeam dimensions are $W = 2.716$ nm, $H = 2.716$ nm, and $L = 26.069$ nm

To assess whether the extracted frequency depends on the excitation amplitude, simulations were performed using three excitation amplitudes, $A = 0.102$, 0.203, and 0.406 Å, for a hollow square silicon nanobeam with length $L = 34.760$ nm, outer dimension $H_{\text{out}} = 4.345$ nm, and inner dimension $H_{\text{in}} = 2.716$ nm. The resulting vibration responses and their corresponding sinusoidal fits are presented in Fig. 3. The vibration responses obtained for the three amplitudes were fitted using the sinusoidal model described above. All three cases yielded the same natural frequency, $\omega \approx 134.56$ Giga rad/s, demonstrating that the extracted natural frequency is independent of excitation amplitude within the range considered. It should also be noted that the frequency obtained using this fitting procedure is identical to that determined using the Fast Fourier Transform (FFT) approach, further confirming the accuracy and robustness of the method.

3 Results and discussions

This section presents the results obtained for the three nanobeam configurations investigated in this study. The first group consists of solid rectangular nanobeams with varying cross-sectional widths. The second group includes hollow square nanobeams with different inner cavity dimensions. The third group comprises hollow circular nanobeams in which the inner diameter is systematically varied.

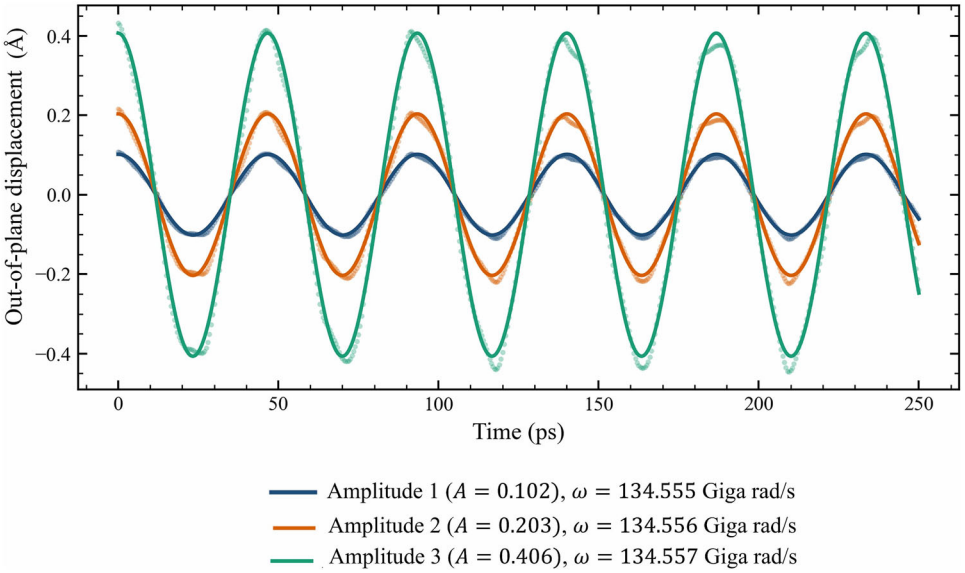

Fig. 3 Time-domain vibration responses of a hollow square silicon nanobeam ($L = 34.760$ nm, $H_{out} = 4.345$ nm, $H_{in} = 2.716$ nm) subjected to three excitation amplitudes ($A = 0.102$, 0.203, and 0.406 Å). MD data are shown together with the corresponding sinusoidal fits used to extract the natural frequency. The fitted responses yield an identical angular frequency of $\omega \approx 134.56$ Giga rad/s for all excitation amplitudes, demonstrating that the natural frequency is independent of excitation amplitude within the investigated range

Table 1 First natural frequencies (ω_{MD}) of silicon nanobeams with varying width W and dimensionless surface-to-volume ratio ($\overline{SVR}$), obtained from MD simulations, and their comparison with predictions of the classical size-independent continuum model (ω_{cont})

Rectangular silicon nanobeams with $H = 2.716$ and $L = 21.724$				
W	$\overline{SVR}$	ω_{MD}	ω_{cont}	$\frac{\omega_{MD}}{\omega_{cont}}$
0.272	178.000	109.537	228.579	0.479
0.543	98.000	158.432	228.579	0.693
0.815	71.333	175.416	228.579	0.767
1.086	58.000	184.806	228.579	0.808
1.629	44.667	194.586	228.579	0.851
2.172	38.000	199.853	228.579	0.874
2.716	34.000	203.274	228.579	0.889
3.259	31.333	205.826	228.579	0.900
3.802	29.428	207.866	228.579	0.909
4.345	28.000	209.534	228.579	0.917

The corresponding frequency ratios ($\frac{\omega_{MD}}{\omega_{cont}}$) are also reported. All nanobeams have an equal thickness of $H = 2.716$ and a length of $L = 21.724$. Frequencies are reported in Giga rad/s, and all dimensions are expressed in nm

3.1 Solid rectangular nanobeams

According to classical Timoshenko beam theory, all nanobeams with identical thickness H and length L are expected to exhibit the same fundamental natural frequency. This is because the natural frequency ω is proportional to H/L^2 and therefore depends only on these two geometric parameters. In Table 1, all rectangular nanobeams have the same thickness $H = 2.716$ nm and length $L = 21.724$ nm; therefore, classical continuum mechanics predicts a constant value of $\omega_{cont} = 228.579 Gigarad/s$ for every width W.

However, the MD results in Table 1 and Fig. 4 reveal substantial deviations from this prediction when the beam dimension becomes small. For the narrowest nanobeam with $W = 0.272$ nm, and accordingly $\overline{SVR} = 178$, the natural frequency drops to $\omega_{MD} = 109.537 Gigarad/s$, corresponding to a frequency ratio ($\frac{\omega_{MD}}{\omega_{cont}}$) of only 0.479. This means the actual frequency is less than half of the classical prediction. As the width increases, the natural frequency increases monotonically, reaching $\omega_{MD} = 209.534 Gigarad/s$ for the widest beam with $W = 4.345$ nm ($\overline{SVR} = 28$), corresponding to a ratio of 0.947.

Figure 4a clearly shows this monotonic increase in $\frac{\omega_{MD}}{\omega_{cont}}$ with increasing width, while Fig. 4b shows the corresponding monotonic decrease in ω_{MD} with increasing $\overline{SVR}$.

This discrepancy between MD and classical predictions arises from size-dependent surface elasticity, which classical continuum theory neglects. As the nanobeam width decreases, $\overline{SVR}$ increases sharply, indicating a larger fraction

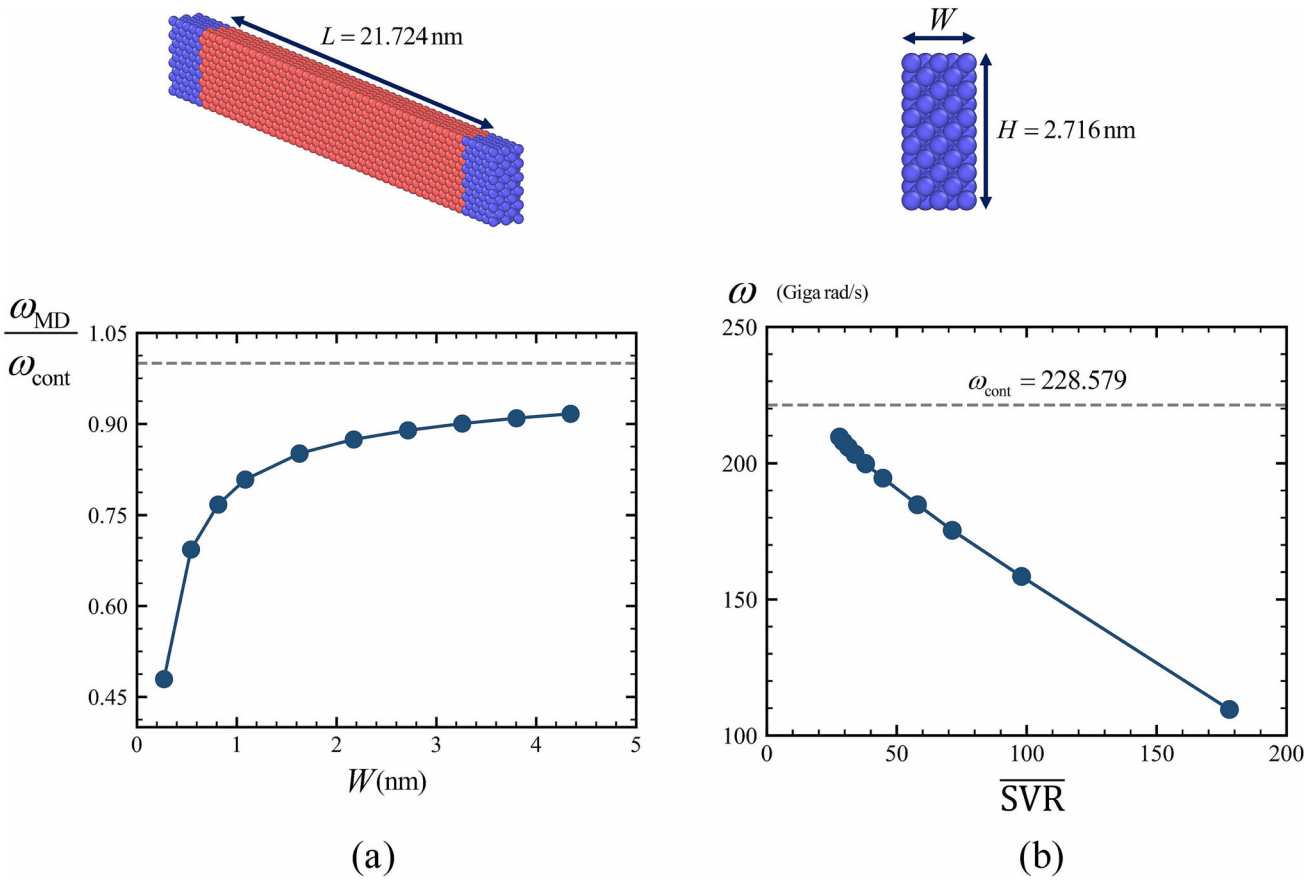

Fig. 4 **a** Frequency ratios ($\frac{\omega_{\text{MD}}}{\omega_{\text{cont}}}$) of silicon nanobeams as a function of width W. **b** MD-derived natural frequencies (ω_{MD}) as a function of dimensionless surface-to volume ratio ($\overline{\text{SVR}}$). All nanobeams have an equal thickness of $H = 2.716$ nm and a length of $L = 21.724$ nm. Frequencies are reported in Giga rad/s

of surface atoms. This increases surface-induced softening, reducing the effective stiffness of the nanobeam and lowering its natural frequency. The narrowest beams, with the highest $\overline{\text{SVR}}$, therefore exhibit the strongest softening. As the width increases and $\overline{\text{SVR}}$ decreases, the proportion of surface atoms becomes smaller, the bulk contribution dominates, and the MD results converge toward the classical prediction.

Figure 4b illustrates this behavior clearly: nanobeams with high $\overline{\text{SVR}}$ exhibit markedly lower natural frequencies due to dominant surface-induced softening, while wider nanobeams with lower $\overline{\text{SVR}}$ approach the classical continuum limit. These results confirm that surface-to-volume ratio is a critical parameter governing the mechanical response of nanoscale beams, and that classical continuum mechanics becomes increasingly inaccurate as SVR increase.

3.2 Hollow square nanobeams

According to classical beam theory, removing material from the core of a beam increases its natural frequency because the reduction in mass is greater than the small decrease in bending stiffness. Since the material at the center contributes very little to the beam's resistance to bending, removing it significantly lightens the structure while maintaining most of its strength. This increases the ratio of stiffness (EI) to mass (m) which directly results in a higher vibration frequency ($\omega \sim \sqrt{\frac{EI}{m}}$). This trend is reflected in the classical frequencies (ω_{cont}) in Table 2, which increase monotonically from $\omega_{cont} = 142.855 Gigarad/s$ for the solid nanobeam ($H_i = 0$) to $\omega_{cont} = 174.259 Gigarad/s$ for the most hollow nanobeam ($H_{\text{in}} = 3.530 nm$).

However, the MD results in Table 2 and Fig. 5 show a non-monotonic trend that classical elasticity cannot capture. Figure 5a illustrates that the frequency ratio $\frac{\omega_{\text{MD}}}{\omega_{\text{cont}}}$ decreases steadily as H_{in} increases. Even in the range where the MD frequency (ω_{MD}) itself rises slightly, the frequency ratio continues to fall because the classical model predicts a much stronger stiffening effect than what actually occurs at the nanoscale. This monotonic decline in the frequency ratio $\frac{\omega_{\text{MD}}}{\omega_{\text{cont}}}$ indicates that surface-induced softening is always present, but its influence is initially dominated by

Table 2 First natural frequencies (ω_{MD}) of hollow-core square nanobeams with varying inner side length H_{in} and dimensionless surface-to-volume ratio ($\overline{SVR}$), obtained from MD simulations, and their comparison with predictions of the classical size-independent continuum model (ω_{cont})

Hollow-core square nanobeams with $H_{out} = 4.345$ and $L = 34.760$				
H_{in}	$\overline{SVR}$	ω_{MD}	ω_{cont}	$\frac{\omega_{MD}}{\omega_{cont}}$
0.000	34.000	132.456	142.855	0.927
0.543	38.571	132.928	143.788	0.924
1.086	44.667	134.153	146.387	0.916
1.629	53.200	135.611	150.729	0.900
2.172	66.000	136.387	156.287	0.873
2.716	87.333	134.602	163.056	0.825
2.987	104.400	131.454	166.473	0.790
3.259	130.000	123.753	170.369	0.726
3.530	172.667	104.787	174.529	0.600

The corresponding frequency ratios ($\frac{\omega_{MD}}{\omega_{cont}}$) are also reported. All nanobeams have an equal outer thickness of $H_{out} = 4.345$ and a length of $L = 34.760$. Frequencies are reported in Giga rad/s, and all dimensions are expressed in nm

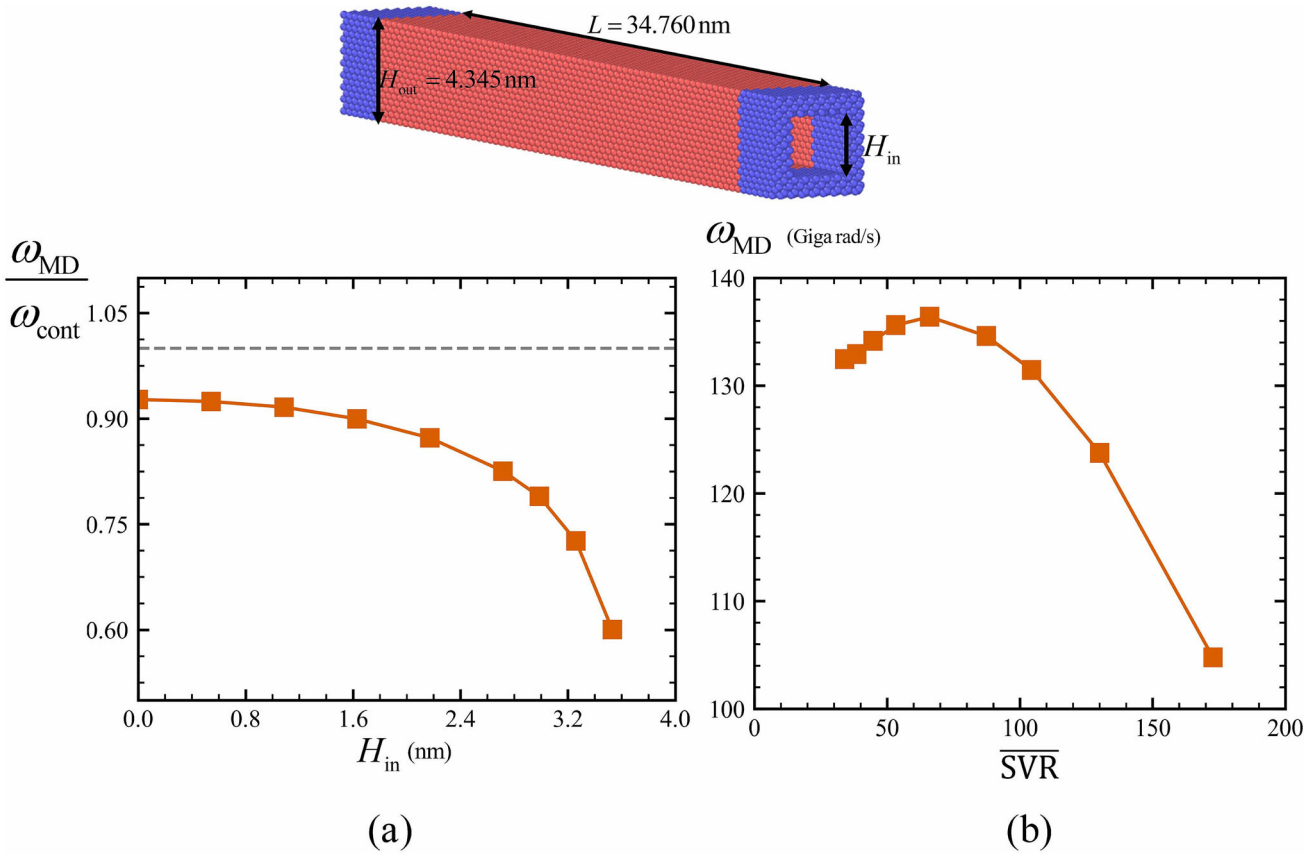

Fig. 5 **a** Frequency ratios ($\frac{\omega_{MD}}{\omega_{cont}}$) of hollow-core square nanobeams with varying inner side lengths H_{in}. **b** MD-derived natural frequencies (ω_{MD}) as a function of $\overline{SVR}$. All nanobeams have an equal outer thickness of $H_{out} = 4.345$ nm and a length of $L = 34.760$ nm. Frequencies are reported in Giga rad/s

bulk-dominated geometric stiffening. As the cavity grows and the surface-to-volume ratio increases, surface effects intensify, causing the frequency ratio to drop more rapidly.

Figure 5b shows the actual MD-predicted natural frequencies (ω_{MD}) as a function of $\overline{SVR}$. Unlike the classical prediction, the MD frequencies exhibit a non-monotonic

trend. As the inner side length H_{in} increases, ω_{MD} first increases slightly, reaches a maximum at $H_{\text{in}} = 2.172$ nm, and then decreases sharply for larger cavities.

For the solid beam ($H_{\text{in}} = 0$), the MD frequency is $\omega_{MD} = 132.456 Gigarad/s$. As the cavity grows to $H_{\text{in}} = 2.172$ nm ($\overline{\text{SVR}} = 66$), the MD frequency increases to $\omega_{MD} = 136.387 Gigarad/s$, representing the peak of the curve. Beyond this point, further increases in cavity size cause a significant decrease in natural frequency, reaching $\omega_{MD} = 104.787 Gigarad/s$ for the most hollow configuration ($H_{\text{in}} = 3.530$ nm, $\overline{\text{SVR}} = 172.667$). This two-trend behavior is illustrated in Fig. 5b, where the MD frequencies first rise and then fall as $\overline{\text{SVR}}$ increases.

This non-monotonic response arises from the competition between bulk stiffness and surface elasticity, which evolves in a complex manner as the cavity grows. For small cavities ($0 \leq H_{\text{in}} < 2.172$ nm), the increase in $\overline{\text{SVR}}$ from 34 to 66 is not yet sufficient for the compliant surface layer to dominate the mechanical response. The remaining bulk material still governs the stiffness, and geometry-induced stiffening outweighs surface-related softening. This explains the slight increase in ω_{MD} from 132.456 to 136.387 Giga rad/s.

At $H_{\text{in}} = 2.172$ nm, the wall thickness has decreased enough for the surface and bulk contributions to become comparable. The MD frequency reaches its maximum at this balance point, where the geometry-induced stiffening and surface-related softening counteract each other.

For larger cavities ($H_{\text{in}} > 2.172$ nm), the wall becomes very thin and the $\overline{\text{SVR}}$ increases sharply from 66 to 172.667. In this regime, the compliant surface layer outweighs bulk-dominated geometric stiffening and becomes the dominant factor in the mechanical response. As a result, the natural frequency decreases rapidly, reaching $\omega_{MD} = 104.787$ Giga rad/s for the most hollow configuration.

3.3 Hollow circular nanobeams

In circular nanobeams, the classical continuum model predicts that increasing the cavity size increase the natural frequency because the mass decreases more rapidly than the bending rigidity. The circular cross-section distributes material uniformly around the neutral axis, so removing material from the center has only a minor effect on stiffness while significantly reducing inertia. This produces a monotonic increase in the classical frequencies (ω_{cont}) which rise from 168.736 Giga rad/s for the solid beam ($D_{\text{in}} = 0$) to 203.336 Giga rad/s for the most hollow configuration ($D_{\text{in}} = 2.444$ nm).

However, the MD results in Table 3 and Fig. 6, reveal a more intricate size-dependent behavior, similar to that reported for hollow square nanobeams. Figure 6a shows that the frequency ratio ($\frac{\omega_{\text{MD}}}{\omega_{\text{cont}}}$) decreases continuously as the cavity expands. Even when the MD frequency (ω_{MD}) itself rises slightly, the frequency ratio still drops because the classical model predicts a much stronger stiffening effect than what actually occurs. This steady decline reflects the persistent influence of surface-related softening, which becomes more pronounced as the surface-to-volume ratio increases. Thus, Fig. 6a demonstrates that classical elasticity increasingly overestimates the stiffness of circular silicon nanobeams as they become more hollow.

Figure 6b provides the direct MD frequencies and shows a clear two-stage trend. For the solid beam, the MD frequency is $\omega_{\text{MD}} = 142.262$ Giga rad/s. As the cavity begins to form, the frequency increases modestly, reaching 145.756 Giga rad/s at $D_{\text{in}} = 1.358$ nm ($\overline{\text{SVR}} = 55.357$). Beyond this point, further increases in cavity size lead to a rapid decline in frequency, falling to 96.409 756 Giga rad/s for the most hollow configuration ($D_{\text{in}} = 2.444$ nm and $\overline{\text{SVR}} = 128.5$).

The observed non-monotonic response results from the interaction between bulk stiffness and surface elasticity, which progressively changes as the cavity size increases. For small cavities, the remaining annular wall is still thick enough that the bulk material governs the bending stiffness. The modest increase in $\overline{\text{SVR}}$ does not yet allow the compliant surface layer to dominate, so the slight geometric stiffening outweighs surface-induced softening. This explains the initial rise in ω_{MD}.

At $D_{\text{in}} = 1.358$ nm, the wall thickness has decreased to the point where the influence of surface atoms becomes comparable to that of the interior. The MD frequency reaches its maximum at this balance point, where the geometric stiffening and the growing surface softening counteract each other.

For larger cavities, the circular wall becomes very thin, and the $\overline{\text{SVR}}$ increases sharply. In this regime, the surface layer governs the mechanical response. Because silicon surfaces possess negative surface elastic constants, the effective stiffness drops rapidly, causing the MD frequency to fall well below the classical prediction. The final value of $\omega_{\text{MD}} = 96.409$ Giga rad/s at $D_{\text{in}} = 2.444$ nm, reflects a regime where surface-dominated softening exceeds any remaining geometric stiffening.

Although the numerical values differ from the hollow square nanobeams, the circular geometry exhibits the same qualitative two-stage behavior, confirming that the transition from bulk-dominated geometric stiffening to surface-dominated softening is a general consequence of increasing surface-to-volume ratio rather than a feature of a particular cross-section.

3.4 Comparison with surface-elasticity theory

To assess whether the non-monotonic frequency response observed above can be predicted from an established surface-elasticity framework, the model of Miller and Shenoy (2000) is applied to the hollow nanobeam geometries. In this model,

Table 3 First natural frequencies (ω_{MD}) of hollow-core circular nanobeams with varying inner diameter (D_{in}) and $\overline{SVR}$, obtained from MD simulations and their comparison with predictions of the classical size-independent continuum model (ω_{cont})

Hollow-core circular nanobeams with $D_{out} = 3.259$ and $L = 26.069$				
D_{in}	$\overline{SVR}$	ω_{MD}	ω_{cont}	$\frac{\omega_{MD}}{\omega_{cont}}$
0	32.500	142.262	168.736	0.843
0.543	38.900	143.374	170.588	0.840
1.086	48.500	144.811	176.601	0.820
1.358	55.357	145.756	180.588	0.807
1.629	64.500	144.177	185.540	0.777
1.901	77.300	142.045	190.934	0.744
2.172	96.500	131.910	196.954	0.670
2.444	128.500	96.409	203.336	0.474

The corresponding frequency ratios are also reported. All nanobeams have an equal outer diameter of $D_{out} = 3.259$ and a length of $L = 26.069$. Frequencies are reported in Giga rad/s, and all dimensions are expressed in nm

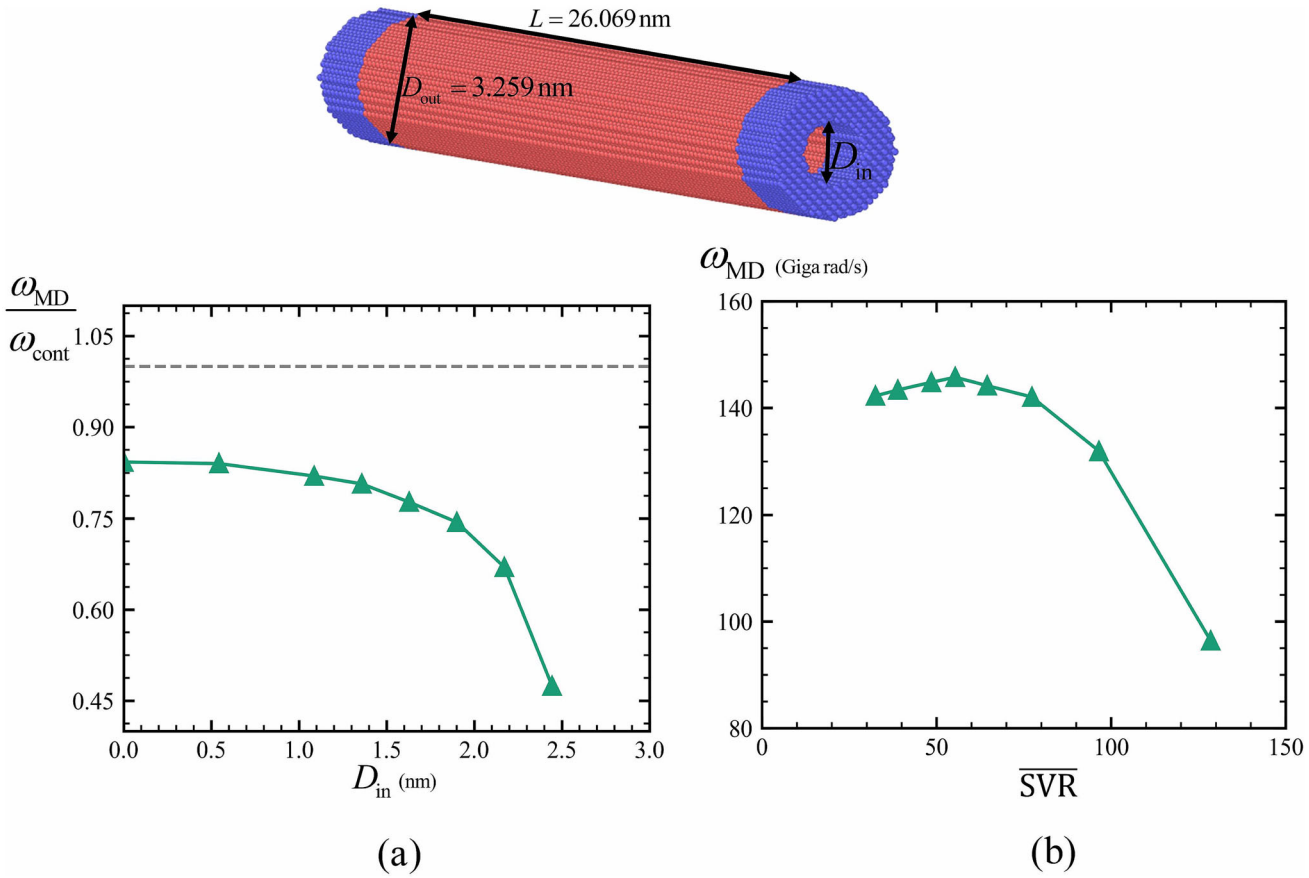

Fig. 6 **a** Frequency ratios ($\frac{\omega_{MD}}{\omega_{cont}}$) of hollow-core circular nanobeams with varying inner diameter D_{in}. **b** MD-derived natural frequencies (ω_{MD}) as a function of $\overline{SVR}$. All nanobeams have an equal outer thickness of $D_{out} = 3.259$ nm and a length of $L = 26.069$ nm. Frequencies are reported in Giga rad/s

the bending moment of a beam including surface effects is given by

$$M = -\frac{1}{\rho}(EI + SK) \tag{8}$$

where E and I are the bulk Young's modulus and moment of inertia, ρ is the radius of curvature, S is the surface elastic modulus, and $K = \int_{\partial A} y^2 dl$ is the surface ("perimeter")

moment of inertia, obtained by integrating y^2 around the boundary of the cross-section rather than over its area.

The perimeter moment of inertia K is given by Eq. (9) for solid rectangular cross-sections, and by Eqs.(10) and (11) for hollow square and hollow circular nanobeams, respectively.

$$K = \frac{1}{2}WH^2 + \frac{1}{6}H^3 \tag{9}$$

$$K = \frac{2}{3}(H_{\text{out}}^3 + H_{\text{in}}^3) \tag{10}$$

$$K = \frac{\pi}{8}(D_{\text{out}}^3 + D_{\text{in}}^3) \tag{11}$$

For a square Si beam loaded along [100], Miller and Shenoy report $E = 0.6673$ eV/Å^3 (106.9 GPa) and $S = -0.7333$ eV/Å^2 (-11.75 N/m), obtained from the bulk constants C_{11}, C_{12} and the surface constants S_{11}, S_{12} of the Si{100}, 1×1 surface. Using these constants, the frequency including the surface correction is estimated as

$$\omega_{\text{MS}} = \omega_{\text{cont}}\sqrt{1 + \frac{SK}{EI}} \tag{12}$$

It is important to note that the atomistic simulations performed in (Miller and Shenoy 2000) were carried out for static, zero-temperature bending of solid silicon bars using an idealized, unreconstructed Si{100} 1×1 surface, whereas the present results are obtained from MD simulations of the dynamic vibration of clamped–clamped nanobeams at $T = 1$ K, including hollow cross-sections that were not considered in the original model. In particular, the surface constants reported by Miller and Shenoy describe the outer {100} facets of a solid bar; in the hollow geometries considered here, the same constants are applied, as a first approximation, to the inner cavity surface as well, even though the local atomic environment and possible relaxation or reconstruction at the cavity wall may differ from that of the outer surface. Given these differences in simulation conditions, boundary conditions, geometry, and surface termination, exact quantitative agreement between the two approaches is not expected. The purpose of this comparison is therefore to check whether the qualitative trend observed in the present work — namely, the non-monotonic dependence of frequency on cavity size — is already contained within an established surface-elasticity framework, rather than to reproduce the absolute frequency values.

Figure 7 compares the MD results with the predictions of the Miller–Shenoy surface-elasticity model for solid, hollow-square, and hollow-circular nanobeams. For the solid beam (Fig. 7a), both approaches predict a monotonic decrease in frequency with increasing $\overline{\text{SVR}}$. The surface-corrected frequencies remain consistently lower than the MD values, but the two datasets exhibit nearly parallel trends over the entire range considered. This agreement indicates that, for solid nanobeams, the dominant effect of the surface elasticity model is to reduce the effective bending stiffness through the negative surface elastic modulus of silicon, leading to a gradual decrease in frequency as the surface contribution becomes increasingly important.

The behavior changes markedly for the hollow geometries. In both the square and circular nanobeams, the MD simulations reveal a non-monotonic dependence of frequency on $\overline{\text{SVR}}$, characterized by an initial increase followed by a decrease as the cavity size grows. Remarkably, the Miller–Shenoy model predicts the same qualitative behavior despite being derived for a much simpler continuum representation of surface elasticity. This result suggests that the frequency maximum is not purely an atomistic phenomenon but arises naturally from the competition between geometric softening and surface-induced stiffening.

For the hollow-square nanobeams (Fig. 7b), the MD frequency reaches a maximum value of 136.387 Giga rad/s at $\overline{\text{SVR}} = 66$, whereas the surface-elasticity prediction reaches its maximum of 138.001 Giga rad/s at the larger value $\overline{\text{SVR}} = 87.3$. Similarly, for the hollow-circular nanobeams (Fig. 7c), the MD peak occurs at $\overline{\text{SVR}} = 55.4$ with a frequency of 145.756 Giga rad/s, while the continuum prediction reaches its maximum at $\overline{\text{SVR}} = 64.5$ with a frequency of 152.581 Giga rad/s. Thus, in both hollow geometries, the continuum model predicts the peak at a somewhat larger cavity size than observed in the MD simulations.

The discrepancy becomes more pronounced at large $\overline{\text{SVR}}$. In the MD results, the frequency decreases more rapidly once the cavity exceeds the optimum size, particularly for the circular nanobeams. The surface-elasticity model, by contrast, predicts a more gradual decline. This difference suggests that atomistic mechanisms not included in the continuum formulation become increasingly important for thin-walled structures. Possible contributors include local stress redistribution around the cavity, changes in atomic coordination, surface relaxation, and geometry-dependent variations in the elastic properties of the inner surface. Because the Miller–Shenoy model treats the surface elastic modulus as a constant and assumes the same surface properties for both the external and internal boundaries, it cannot capture such effects.

Overall, the comparison demonstrates that the Miller–Shenoy surface-elasticity framework successfully captures the essential physics responsible for the non-monotonic frequency response of hollow silicon nanobeams. Although quantitative differences remain, particularly regarding the precise location and magnitude of the frequency maximum, the model reproduces the key trend observed in the MD simulations. This agreement supports the interpretation that the frequency peak originates from

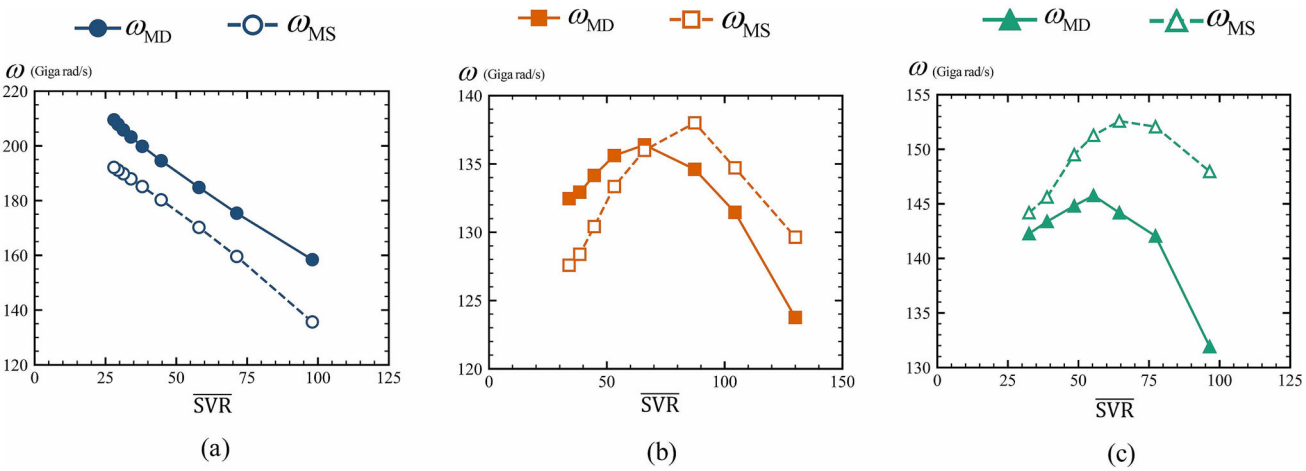

Fig. 7 **a** Comparison of the MD natural frequencies, ω_{MD}, and the Miller–Shenoy surface-corrected predictions, ω_{MS} (Eq. (12)), as a function of the dimensionless surface-to-volume ratio, $\overline{SVR}$, for **a** solid rectangular nanobeams ($H = 2.716$ nm, $L = 21.724$ nm), **b** hollow-core square nanobeams ($H = 4.345$ nm, $L = 34.760$ nm), and **c** hollow-core circular nanobeams ($D = 3.259$ nm, $L = 26.069$ nm). Frequencies are reported in Giga rad/s

the competition between increasing surface effects and decreasing bulk bending rigidity as the cavity size grows.

3.5 Scaling of geometric–surface competition

The previous section showed that the surface-elasticity formulation of Miller and Shenoy reproduces the non-monotonic frequency response of hollow nanobeams. Here, the stiffening-to-softening transition is expressed in terms of a dimensionless geometric parameter derived from the perimeter moment of inertia in Eqs. (9, 10, 11), and compared with the present MD results.

For the hollow square nanobeam, substituting the bulk moment of inertia, $I = (H_{\text{out}}^4 - H_{\text{in}}^4)/12$, and the perimeter moment of inertia, $K = \frac{2}{3}(H_{\text{out}}^3 + H_{\text{in}}^3)$, into the surface-correction ratio SK/EI appearing in Eq. (12), gives

$$\frac{SK}{EI} = \frac{8S}{E}\frac{H_{\text{out}}^3 + H_{\text{in}}^3}{H_{\text{out}}^4 - H_{\text{in}}^4} \tag{13}$$

Introducing the dimensionless cavity ratio $\xi = \frac{H_{in}}{H_{out}}$ and factoring H_{out} out of the numerator and denominator reduces Eq. (13) to

$$\frac{SK}{EI} = \frac{8S}{EH_{\text{out}}}\frac{1+\xi^3}{1-\xi^4} \tag{14}$$

Recognizing S/E as the intrinsic material length scale h_0 introduced by (Miller and Shenoy 2000), Eq. (14) can be written compactly as

$$\frac{SK}{EI} = 8\left(\frac{h_0}{H_{\text{out}}}\right) f(\xi) \tag{15}$$

where

$$f(\xi) = \frac{1+\xi^3}{1-\xi^4} \tag{16}$$

An identical derivation, carried out for the hollow circular cross-section with $\xi = \frac{D_{in}}{D_{out}}$, yields the same relation and the same function $f(\xi)$, despite the two derivations proceeding from entirely different coefficients in K and I. Equation (15) therefore generalizes to both geometries:

$$\frac{SK}{EI} = 8\left(\frac{h_0}{\Lambda}\right) f(\xi) \tag{17}$$

where $\Lambda = H_{\text{out}}$ for the hollow square beam and $\Lambda = D_{\text{out}}$ for the hollow circular beam. This result shows that the surface-softening contribution depends on cross-sectional shape only through the single outer dimension Λ, and is otherwise governed by a single, geometry-independent function of the cavity ratio $f(\xi)$.

The classical, surface-elasticity-free frequency satisfies $\omega_{cont}^2 \sim \frac{I}{A}$ for fixed length, density, and boundary condition. For the hollow square cross-section, with $A = H_{\text{out}}^2 - H_{\text{in}}^2$,

$$\frac{I}{A} = \frac{H_{\text{out}}^2 + H_{\text{in}}^2}{12} \tag{18}$$

By introducing $\xi = \frac{H_{in}}{H_{out}}$ in the Eq. (18), the following expression in terms of ξ is obtained:

$$\frac{I}{A} = \frac{H_{\text{out}}^2}{12}(1+\xi^2) \tag{19}$$

Normalizing by the corresponding solid-beam value defines the dimensionless geometric-stiffening function

$$g(\xi) = \frac{\omega_{\text{cont}}^2(\xi)}{\omega_0^2} = \frac{(I/A)(\xi)}{(I/A)(0)} = 1 + \xi^2 \tag{20}$$

where ω_0 denotes the natural frequency of the corresponding solid beam ($\xi = 0$). An identical functional form is obtained for the hollow circular cross-section by the same algebraic procedure.

Squaring Eq. (12),

$$\omega_{\text{MS}}^2 = \omega_{\text{cont}}^2(1 + \frac{SK}{EI}) \tag{21}$$

and dividing both sides by ω_0^2 gives

$$(\frac{\omega_{\text{MS}}}{\omega_0})^2 = (\frac{\omega_{\text{cont}}}{\omega_0})^2 (1 + \frac{SK}{EI}) \tag{22}$$

Substituting Eq. (17) and (20) into Eq. (22), yields a two-term scaling relation as follows:

$$(\frac{\omega_{\text{MS}}}{\omega_0})^2 = (1 + \xi^2)\left[1 + 8\,\frac{h_0}{\Lambda}\, f(\xi)\right] \tag{23}$$

In Eq. (23), the geometric factor $g(\xi) = 1 + \xi^2$ increases monotonically with ξ, reflecting bulk-dominated stiffening, whereas the bracketed surface term decreases monotonically because $h_0 < 0$ for silicon along the [100] orientation. The non-monotonic frequency response therefore emerges from the competition between a rising and a falling factor, rather than from either mechanism in isolation.

The stationary point of Eq. (23) obtained by numerically solving $d(\omega/\omega_0)^2/d\xi = 0$, has no closed-form solution, since the resulting condition is transcendental. The predicted transition location, ξ^*, is consequently expressed as a function of the single dimensionless parameter h_0/Λ. For the beam dimensions considered here ($H_{\text{out}} = 4.345$ nm, $D_{\text{out}} = 3.259$ nm), this procedure predicts $\xi^* = 0.628$ ($H_{\text{in}} \approx 2.73$ nm) for the hollow square beam and $\xi^* = 0.559$ ($D_{\text{in}} \approx 1.82$ nm) for the hollow circular beam. These two values differ because the corresponding beams have different outer dimensions Λ, and therefore different values of h_0/Λ. Equation (23) is a single, unified expression that returns the appropriate ξ^* for any value of Λ, including outer dimensions beyond those examined in the present simulations.

Figure 8 tests Eqs. (16), (17), (20) and (23) directly against the MD and surface-corrected results of Sect. 3.4 in three parts. Figure 8a shows the normalized surface-correction term $\left[(\omega/\omega_{\text{cont}})^2 - 1\right]/(8h_0/\Lambda)$, computed from ω_{MS}, as a function of ξ. Data for hollow square and circular geometries collapse onto $f(\xi)$, consistent with Eq. (16). This collapse is a direct consequence of the formulation and therefore constitutes a consistency check.

Figure 8b shows the normalized results obtained using MD frequencies ω_{MD} in place of ω_{MS}. Both geometries exhibit a monotonically increasing dependence on ξ, consistent with a common surface-softening mechanism. The two datasets do not collapse onto a single curve. This discrepancy suggests a cross-section-dependent contribution to the atomistic surface response not captured by the linear, perimeter-based formulation in Eq. (16), e.g., a sensitivity to local cavity-wall curvature, which differs systematically between square and circular geometries. A definitive explanation would require a dedicated atomistic analysis of the cavity-wall structure and is deferred to future work. More generally, the results indicate that the proposed dimensionless grouping correctly identifies the governing scaling variable for cavity-size dependence, while the atomistic surface response deviates from the linear, geometry-independent assumption of Eq. (16), particularly at small-to-intermediate cavity ratios.

Figure 8c plots Eq. (23) directly, together with the corresponding ω_{MS}^2/ω_0^2 and ω_{MD}^2/ω_0^2 data for both geometries. The surface-corrected results follow the Eq. (23) predictions closely, as expected from their shared analytical origin. The MD results exhibit a similar rise-and-fall trend over the same range of ξ, but with maxima shifted to lower values of ξ. Specifically, the peak occurs at $\xi^* = 0.5$ for the hollow square geometry and at $\xi^* \approx 0.417$ for the hollow circular geometry, compared with the theoretical predictions $\xi^* = 0.628$ and $\xi^* = 0.559$, respectively.

Overall, Eq. (23) provides a minimal two-term scaling relation in which a geometric contribution, $g(\xi) = 1 + \xi^2$, competes against a surface contribution governed by the intrinsic material length $h_0 = S/E$, normalized by the characteristic outer dimension Λ. Because h_0 is a fixed material property, Eq. (23) predicts how the stiffening-to-softening transition shifts as Λ varies: increasing Λ reduces $|\, h_0/\Lambda \,|$ and shifts the predicted transition toward larger ξ. This relation thus provides a basis for extrapolating the present findings to beam dimensions beyond those simulated here.

4 Limitations and future directions

Several limitations of the present study should be acknowledged. First, the analysis was restricted to single-crystal silicon nanobeams oriented along the [100] crystallographic direction. Because surface elastic properties depend on both material type and crystal orientation, the quantitative location of the transition between geometric stiffening and surface-dominated softening may differ for other materials and orientations. Future studies should therefore investigate whether the observed non-monotonic vibrational behavior

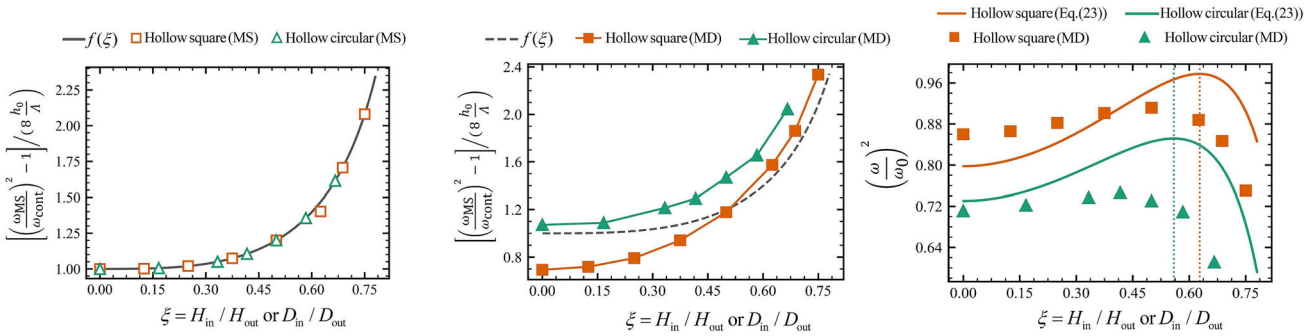

Fig. 8 Dimensionless scaling analysis of the competition between geometric stiffening and surface softening. **a** Normalized surface-correction term $\left[\left(\frac{\omega_{MS}}{\omega_{cont}}\right)^2 - 1\right]/(8\,\frac{h_0}{\Lambda})$, computed from the Miller–Shenoy surface-corrected frequencies ω_{MS}, showing the exact collapse onto the theoretical function $f(\xi)$ predicted by Eq. (16) for both hollow geometries. **b** Normalized MD frequency data, $\left[\left(\frac{\omega_{MD}}{\omega_{cont}}\right)^2 - 1\right]/(8\,\frac{h_0}{\Lambda})$, plotted as a function of ξ together with the theoretical function $f(\xi)$. (c) Squared frequency ratio, ω^2/ω_0^2, as a function of ξ. Symbols denote the MD frequencies ω_{MD} and the Miller–Shenoy frequencies ω_{MS}; the solid line represents the prediction of the full two-term scaling relation, Eq. (23). Here, ω_0 denotes the frequency of the corresponding solid beam ($\xi = 0$)

persists across different crystalline materials and surface orientations.

Second, the MD simulations were performed using the SW interatomic potential. Although this potential has been extensively validated for silicon and has been widely used to investigate its mechanical properties, quantitative predictions may vary when alternative interatomic potentials are employed. A systematic comparison between different potential models could provide additional insight into the sensitivity of the predicted transition behavior.

Third, all simulations were conducted at a low temperature in order to minimize thermal fluctuations and facilitate accurate frequency extraction. Consequently, temperature-dependent effects such as anharmonicity, thermal expansion, and thermally induced surface relaxation were not considered. Investigating the influence of temperature on the competition between geometric and surface effects remains an important topic for future research.

The present work was limited to the free transverse vibration of nanobeams and focused exclusively on the fundamental bending mode. While the observed non-monotonic frequency response was interpreted as a consequence of the competition between geometric stiffening and surface-induced softening, it remains unclear whether the same mechanism governs other mechanical responses. In particular, static bending behavior deserves further investigation, since surface elasticity theories such as that of Miller and Shenoy were originally developed in the context of bending deformation. Future studies could therefore examine the size-dependent bending stiffness and deflection of hollow nanobeams to determine whether a similar stiffening-to-softening transition exists under static loading and whether the scaling framework proposed in the present work remains applicable beyond vibrational phenomena.

Finally, only hollow square and hollow circular cross-sections were investigated. Extending the analysis to other hollow geometries and conducting experimental validation of the predicted non-monotonic behavior would provide further insight into the interplay between geometric stiffening and surface-induced softening. A particularly important direction for future research is the atomistic characterization of cavity-wall surfaces to determine how local curvature, atomic coordination, and surface relaxation influence the effective surface elasticity of hollow nanostructures and the location of the stiffening-to-softening transition.

5 Conclusions

This study employed MD simulations to systematically examine the influence of surface-to-volume ratio (SVR) on the size-dependent free transverse vibration of solid and hollow silicon nanobeams. By varying beam width in solid nanobeams and cavity size in hollow square and circular nanobeams, the role of SVR was isolated and directly correlated with deviations from classical continuum predictions.

For solid rectangular nanobeams, the natural frequency decreases monotonically as SVR increases. As the beam width becomes smaller, the fraction of surface atoms grows substantially, and the resulting surface-induced softening reduces the effective bending stiffness. Consequently, the frequencies obtained from atomistic simulations fall below the classical Timoshenko predictions, with the discrepancy becoming more pronounced at high SVR.

Hollow nanobeams exhibit a qualitatively different response. The introduction of a small cavity leads to an initial increase in natural frequency due to bulk-dominated geometric stiffening, where the redistribution of material away from the neutral axis enhances bending rigidity. As the cavity enlarges and the wall thickness decreases, the SVR rises sharply and surface elasticity becomes dominant, producing a significant reduction in natural frequency.

Although the numerical values differ between the square and circular hollow cross-sections, both geometries display the same qualitative transition, indicating that the underlying mechanism is governed by the interplay between bulk stiffness and surface elasticity rather than by cross-sectional shape. This two-stage behavior is captured quantitatively by extending the Miller–Shenoy surface-elasticity framework to hollow geometries and by a dimensionless scaling law that expresses the stiffening-to-softening transition as a competition between a geometric term and a surface term governed by the ratio of the intrinsic material length scale to the beam's outer dimension. Beyond reproducing the qualitative trend observed in the MD simulations, this scaling relation provides a basis for predicting how the transition shifts with beam size, offering a practical, extensible tool for guiding the design of nanoscale resonant devices incorporating hollow silicon elements.

Author contributions A.H. conceived the study, developed the computational methodology, performed the numerical analyses, prepared the figures, wrote the original draft of the manuscript, revised the manuscript, and interpreted the results. H.M.S. contributed to the analytical framework and theoretical derivations, revised the manuscript, and interpreted the results. Both authors approved the final version.

Funding This research did not receive any specific grant from funding agencies in the public, commercial, or not-for-profit sectors.

Data availability The datasets generated and/or analysed during the current study are available from the authors on reasonable request.

Declarations

Conflict of interest The authors declare that they have no known competing financial interests or personal relationships that could have appeared to influence the work reported in this paper.

Declaration of AI-Assisted editing Artificial intelligence tools were used for language editing and proofreading. The authors reviewed and validated all revisions and retained full responsibility for the content, accuracy, and integrity of the manuscript.

References

Abazari AM, Safavi SM, Rezazadeh G, Villanueva LG (2015) Modelling the size effects on the mechanical properties of micro/nano structures. Sensors (Basel) 15:28543–28562. https://doi.org/10.3390/s151128543

Altenbach H, Eremeyev VA (2011) On the shell theory on the nanoscale with surface stresses. Int J Eng Sci 49:1294–1301. https://doi.org/10.1016/j.ijengsci.2011.03.011

Anderson RC, Muller RS, Tobias CW (1994) Porous polycrystalline silicon: a new material for MEMS. J Microelectromech Syst 3:10–18. https://doi.org/10.1109/84.285719

Avramov K, Myrzaliyev D, Urniaieva I, et al (2024) Influence of surface effect on linear vibrations of multi-walled nanoshell. In: 2024 IEEE 5th KhPI Week on Advanced Technology (KhPIWeek), pp 1–6

Baskes MI (1992) Modified embedded-atom potentials for cubic materials and impurities. Phys Rev B 46:2727–2742. https://doi.org/10.1103/PhysRevB.46.2727

Bazant MZ, Kaxiras E, Justo JF (1997) Environment-dependent interatomic potential for bulk silicon. Phys Rev B 56:8542–8552. https://doi.org/10.1103/PhysRevB.56.8542

Bhushan B (2017) Introduction to nanotechnology. In: Bhushan B (ed) Springer handbook of nanotechnology. Springer, Berlin, Heidelberg, pp 1–19

Bochkarev AO, Grekov MA (2019) Influence of surface stresses on the nanoplate stiffness and stability in the Kirsch problem. Phys Mesomech 22:209–223. https://doi.org/10.1134/S1029959919030068

Cammarata RC (1994) Surface and interface stress effects in thin films. Prog Surf Sci 46:1–38. https://doi.org/10.1016/0079-6816(94)90005-1

Cammarata RC (1997) Surface and interface stress effects on interfacial and nanostructured materials. Mater Sci Eng A 237:180–184. https://doi.org/10.1016/S0921-5093(97)00128-7

Cao G, Chen X (2008) Size dependence and orientation dependence of elastic properties of ZnO nanofilms. Int J Solids Struct 45:1730–1753. https://doi.org/10.1016/j.ijsolstr.2007.10.019

Chen J, Wise KD, Hetke JF, Bledsoe SC (1997) A multichannel neural probe for selective chemical delivery at the cellular level. IEEE Trans Biomed Eng 44:760–769. https://doi.org/10.1109/10.605435

Chen J, Zhang G, Li B (2010) Remarkable reduction of thermal conductivity in silicon nanotubes. Nano Lett 10:3978–3983. https://doi.org/10.1021/nl101836z

Chen J, Zhang G, Li B (2011) A universal gauge for thermal conductivity of silicon nanowires with different cross sectional geometries. J Chem Phys 135:204705. https://doi.org/10.1063/1.3663386

Chen M, Pethö L, Sologubenko AS et al (2020) Achieving micron-scale plasticity and theoretical strength in silicon. Nat Commun 11:2681. https://doi.org/10.1038/s41467-020-16384-5

Chowdhury R, Adhikari S, Scarpa F (2011) Vibration of ZnO nanotubes: a molecular mechanics approach. Appl Phys A 102:301–308. https://doi.org/10.1007/s00339-010-5995-3

Craighead HG (2000) Nanoelectromechanical systems. Science 290:1532–1535. https://doi.org/10.1126/science.290.5496.1532

Cuenot S, Frétigny C, Demoustier-Champagne S, Nysten B (2004) Surface tension effect on the mechanical properties of nanomaterials measured by atomic force microscopy. Phys Rev B 69:165410. https://doi.org/10.1103/PhysRevB.69.165410

Cui Y, Wei Q, Park H, Lieber CM (2001) Nanowire nanosensors for highly sensitive and selective detection of biological and chemical species. Science 293:1289–1292. https://doi.org/10.1126/science.1062711

Cui Y, Zhong Z, Wang D et al (2003) High performance silicon nanowire field effect transistors. Nano Lett 3:149–152. https://doi.org/10.1021/nl0258751

Dingreville R, Qu J, Cherkaoui M (2005) Surface free energy and its effect on the elastic behavior of nano-sized particles, wires and films. J Mech Phys Solids 53:1827–1854. https://doi.org/10.1016/j.jmps.2005.02.012

Du X, Zhao H, Zhang L et al (2015) Molecular dynamics investigations of mechanical behaviours in monocrystalline silicon due to nanoindentation at cryogenic temperatures and room temperature. Sci Rep 5:16275. https://doi.org/10.1038/srep16275

Eremeyev VA, Wiczenbach T (2020) On effective bending stiffness of a laminate nanoplate considering Steigmann–Ogden surface elasticity. Appl Sci 10:7402. https://doi.org/10.3390/app10217402

Fu M, Shi Z, Bošnjak B et al (2025) Silicon-based MEMS/NEMS empowered by graphene: a scheme for large tunability and functionality. Microsyst Nanoeng 11:116. https://doi.org/10.1038/s41378-025-00960-0

Gurtin ME, Ian Murdoch A (1975) A continuum theory of elastic material surfaces. Arch Rational Mech Anal 57:291–323. https://doi.org/10.1007/BF00261375

Gurtin ME, Weissmüller J, Larché F (1998) A general theory of curved deformable interfaces in solids at equilibrium. Philos Mag A Phys Condens Matter Struct Defects Mech Prop 78:1093–1109. https://doi.org/10.1080/01418619808239977

Hassanpour A, Darban H (2025) Softening and stiffening size effects in free flexural vibration of small-scale cracked beams. J Sound Vib 612:119135. https://doi.org/10.1016/j.jsv.2025.119135

Hassanpour A, Darban H (2026) Uncovering size effects in crack compliance in nanobeams using MD simulations. Int J Mech Sci 326:111894. https://doi.org/10.1016/j.ijmecsci.2026.111894

He J, Lilley CM (2008a) Surface stress effect on bending resonance of nanowires with different boundary conditions. Appl Phys Lett 93:263108. https://doi.org/10.1063/1.3050108

He J, Lilley CM (2008b) Surface effect on the elastic behavior of static bending nanowires. Nano Lett 8:1798–1802. https://doi.org/10.1021/nl0733233

He LH, Lim CW, Wu BS (2004) A continuum model for size-dependent deformation of elastic films of nano-scale thickness. Int J Solids Struct 41:847–857. https://doi.org/10.1016/j.ijsolstr.2003.10.001

Huang Y, Duan X, Cui Y et al (2001) Logic gates and computation from assembled nanowire building blocks. Science 294:1313–1317. https://doi.org/10.1126/science.1066192

Ilgamov MA, Aitbaeva AA, Pavlov IS, Dmitriev SV (2024) Carbon nanotube under pulsed pressure. Facta Univ Ser Mech Eng 22:275–292. https://doi.org/10.22190/FUME230820049I

Jiang B, Huang S, Zhang J, Su Y (2020) Analysis of frequency drift of silicon MEMS resonator with temperature. Micromachines. https://doi.org/10.3390/mi12010026

Jiang J, Tang F, Gu S et al (2025) Vibration study of functionally graded microcantilever beams in fluids based on modified couple stress theory by considering the physical neutral plane. Int J Str Stab Dyn 25:2550109. https://doi.org/10.1142/S0219455425501093

Kim Y-J, Son K, Choi I-C et al (2011) Exploring nanomechanical behavior of silicon nanowires: AFM bending versus nanoindentation. Adv Funct Mater 21:279–286. https://doi.org/10.1002/adfm.201001471

Langfelder G, Bestetti M, Gadola M (2021) Silicon MEMS inertial sensors evolution over a quarter century. J Micromech Microeng 31:084002. https://doi.org/10.1088/1361-6439/ac0fbf

Lee W-J, Chang J-G, Ju S-P et al (2011) Structure-dependent mechanical properties of ultrathin zinc oxide nanowires. Nanoscale Res Lett 6:352. https://doi.org/10.1186/1556-276X-6-352

Lee HJ, Choi N, Yoon E-S, Cho I-J (2018) MEMS devices for drug delivery. Adv Drug Deliv Rev 128:132–147. https://doi.org/10.1016/j.addr.2017.11.003

Limkatanyu S, Sae-Long W, Rungamornrat J et al (2025) Static bending analysis of nanobeam-substrate medium systems incorporating mixture stress-driven nonlocality, surface energy, and substrate-structure interactions. J Appl Comput Mech 11:327–343. https://doi.org/10.22055/jacm.2024.47226.4679

Love A (1892) A treatise on the mathematical theory of elasticity. Courier Corporation of India

Miller RE, Shenoy VB (2000) Size-dependent elastic properties of nanosized structural elements. Nanotechnology 11:139. https://doi.org/10.1088/0957-4484/11/3/301

Najmi L, Hu Z (2024) Molecular dynamics simulations of effects of geometric parameters and temperature on mechanical properties of single-walled carbon nanotubes. J Compos Sci 8:293. https://doi.org/10.3390/jcs8080293

Pakzad SZ, Esfahani MN, Alaca BE (2024) Investigation of the bending behavior in silicon nanowires: a nanomechanical modeling perspective. Int J Appl Mech 16:2450073. https://doi.org/10.1142/S175882512450073X

Pan H, Feng YP (2008) Semiconductor nanowires and nanotubes: effects of size and surface-to-volume ratio. ACS Nano 2:2410–2414. https://doi.org/10.1021/nn8004872

Park SH, Kim JS, Park JH et al (2005) Molecular dynamics study on size-dependent elastic properties of silicon nanocantilevers. Thin Solid Films 492:285–289. https://doi.org/10.1016/j.tsf.2005.06.056

Plimpton S (1995) Fast parallel algorithms for short-range molecular dynamics. J Comput Phys 117:1–19. https://doi.org/10.1006/jcph.1995.1039

Roduner E (2006) Size matters: why nanomaterials are different. Chem Soc Rev 35:583–592. https://doi.org/10.1039/B502142C

Sadeghian H, Yang C-K, Goosen JFL et al (2010) Effects of size and defects on the elasticity of silicon nanocantilevers. J Micromech Microeng 20:064012. https://doi.org/10.1088/0960-1317/20/6/064012

Sahmani S, Fattahi AM, Ahmed NA (2020) Surface elastic shell model for nonlinear primary resonant dynamics of FG porous nanoshells incorporating modal interactions. Int J Mech Sci 165:105203. https://doi.org/10.1016/j.ijmecsci.2019.105203

Shariati A, Jung D, Mohammad-Sedighi H et al (2020) On the vibrations and stability of moving viscoelastic axially functionally graded nanobeams. Materials (Basel) 13:1707. https://doi.org/10.3390/ma13071707

Sohn Y-S, Park J, Yoon G et al (2009) Mechanical properties of silicon nanowires. Nanoscale Res Lett 5:211–216. https://doi.org/10.1007/s11671-009-9467-7

Stillinger FH, Weber TA (1985) Computer simulation of local order in condensed phases of silicon. Phys Rev B 31:5262–5271. https://doi.org/10.1103/PhysRevB.31.5262

Stukowski A (2009) Visualization and analysis of atomistic simulation data with OVITO–the open visualization tool. Model Simul Mater Sci Eng 18:015012. https://doi.org/10.1088/0965-0393/18/1/015012

Tang F, He S, Shi S et al (2024) Mechanical behavior of nanocircular plates under coupled surface and nonlocal effects by using molecular dynamics simulations. Phys Lett A 500:129380. https://doi.org/10.1016/j.physleta.2024.129380

Tersoff J (1988) Empirical interatomic potential for silicon with improved elastic properties. Phys Rev B 38:9902–9905. https://doi.org/10.1103/PhysRevB.38.9902

Wang KF, Wang BL (2011) Combining effects of surface energy and non-local elasticity on the buckling of nanoplates. Micro Nano Lett 6:941–943. https://doi.org/10.1049/mnl.2011.0458

Wong EW, Sheehan PE, Lieber CM (1997) Nanobeam mechanics: elasticity, strength, and toughness of nanorods and nanotubes. Science 277:1971–1975. https://doi.org/10.1126/science.277.5334.1971

Xu Y, Lin T-HA, Yan P (2025) Design and static analysis of mems-actuated silicon nitride waveguide optical switch. Micromachines. https://doi.org/10.3390/mi16080854

Zare Pakzad S, Nasr Esfahani M, Tasdemir Z et al (2021) A new characterization approach to study the mechanical behavior of silicon nanowires. MRS Adv 6:500–505. https://doi.org/10.1557/s43580-021-00117-x

Zare Pakzad S, Nasr Esfahani M, Tasdemir Z et al (2023) Nanomechanical modeling of the bending response of silicon nanowires. ACS Appl Nano Mater 6:15465–15478. https://doi.org/10.1021/acsanm.3c02077

Zhang Y, Ebata K, Iimori M et al (2025) Uncooled, broadband terahertz bolometers using SOI MEMS beam resonators with piezoresistive readout. Microsyst Nanoeng 11:132. https://doi.org/10.1038/s41378-025-00996-2

Zhou LG, Huang H (2004) Are surfaces elastically softer or stiffer? Appl Phys Lett 84:1940–1942. https://doi.org/10.1063/1.1682698

Zhou RL, Zuo RZ, Wang L et al (2011) Size- and surface-dependent electronic structures of crystalline SiC nanotubes. J Appl Phys 109:084318. https://doi.org/10.1063/1.3567114

Zhu J, Liu X, Shi Q et al (2020) Development trends and perspectives of future sensors and MEMS/NEMS. Micromachines (Basel) 11:7. https://doi.org/10.3390/mi11010007